Geophys. J. Int. (2003) **154,** 146–153

A perfectly matched layer absorbing boundary condition for the second-order seismic wave equation

Dimitri Komatitsch and Jeroen Tromp

Seismological Laboratory, California Institute of Technology, Pasadena, CA 91125, *USA. E-mail: komatits@gps.caltech.edu*

Accepted 2003 January 31. Received 2003 January 29; in original form 2002 September 9

SUMMARY

The perfectly matched layer absorbing boundary condition has proven to be very efficient for the elastic wave equation written as a first-order system in velocity and stress. We demonstrate how to use this condition for the same equation written as a second-order system in displacement. This facilitates use in the context of numerical schemes based upon such a system, e.g. the finite-element method, the spectral-element method and some finite-difference methods. We illustrate the efficiency of this second-order perfectly matched layer based upon 2-D benchmarks with body and surface waves.

Key words: absorbing conditions, elastic waves, perfectly matched layer, seismic modelling, seismic wave propagation, surface waves.

1 INTRODUCTION

In the context of numerical modelling of seismic wave propagation in unbounded media, energy needs to be absorbed at the artificial boundaries of the finite model domain. Such absorbing conditions are relevant for modelling strong ground motion, and for local, regional and continental-scale simulations.

Over the last three decades, numerous techniques have been developed for this purpose: damping layers or 'sponge zones' (e.g. Cerjan *et al.* 1985; Sochacki *et al.* 1987), paraxial conditions (e.g. Clayton & Engquist 1977; Engquist & Majda 1977; Stacey 1988; Higdon 1991; Quarteroni *et al.* 1998), optimized conditions (e.g. Peng & Töksoz 1995), exact absorbing conditions on a spherical contour (e.g. Grote 2000), or asymptotic local or non-local operators (e.g. Givoli 1991; Hagstrom & Hariharan 1998). Unfortunately, all of the local conditions behave poorly under some circumstances, e.g. typically reflect a large amount of spurious energy at grazing incidence or low-frequency energy at all angles of incidence. On the other hand, non-local conditions are difficult to implement and numerically expensive. In the context of electromagnetics, Bérenger (1994) introduced a new condition called the perfectly matched layer (PML), which has the remarkable property of having a zero reflection coefficient for all angles of incidence and all frequencies before discretization (hence the name 'perfectly matched'). This formulation has proven to be extremely efficient compared with classical conditions, and has become very popular. The formulation has been extended to 3-D problems (e.g. Chew & Weedon 1994; Bérenger 1996) and reformulated in a simpler manner in terms of a split field with complex coordinate stretching (e.g. Chew & Weedon 1994; Collino & Monk 1998b). The PML has become very successful in many other fields, e.g. linearized Euler equations (Hesthaven 1998), eddy-current problems (Kosmanis *et al.* 1999) and wave propagation in poroelastic media (Zeng *et al.* 2001).

In the context of wave propagation, the PML has been applied to both acoustic (e.g. Liu & Tao 1997; Qi & Geers 1998; Hagstrom 1999) and elastic problems (e.g. Chew & Liu 1996; Hastings *et al.* 1996; Collino & Monk 1998a; Collino & Tsogka 2001; Basu & Chopra 2003; Cohen & Fauqueux 2003). Collino & Tsogka (2001) demonstrated the high efficiency of the condition compared with the paraxial treatment of Higdon (1991), even though the PML reflection coefficient is not zero after discretization (e.g. Collino & Monk 1998a). All of these papers use the PML in the context of the elastic wave equation formulated as a first-order system in velocity and stress. Unfortunately, this means that this classical PML cannot be used in a straightforward manner in the context of numerical schemes that are based on the wave equation written as a second-order system in displacement, such as most finite-element methods (e.g. Bao *et al.* 1998), the spectral-element method (e.g. Komatitsch & Vilotte 1998; Komatitsch & Tromp 1999), and some finite-difference methods (e.g. Moczo *et al.* 2001). The goal of this article is to reformulate the classical PML condition in order to use it in this context. We also confirm that the PML is highly efficient for the absorption of surface waves, as suggested by Collino & Tsogka (2001).

2 A PML FORMULATION FOR SECOND-ORDER SYSTEMS

The differential or 'strong' form of the elastic wave equation can be written as

$$\rho \partial_t^2 \mathbf{s} = \boldsymbol{\nabla} \cdot (\mathbf{c} : \boldsymbol{\nabla} \mathbf{s}), \tag{1}$$

where $\mathbf{s}$ is the displacement vector, $\boldsymbol{c}$ is the elastic tensor and ρ is the density. The frequency-domain form is

$$-\rho \omega^2 \mathbf{s} = \boldsymbol{\nabla} \cdot (\mathbf{c} : \boldsymbol{\nabla} \mathbf{s}), \tag{2}$$

where ω denotes angular frequency. In a homogeneous, isotropic medium, this equation permits plane-wave solutions of the form $\mathbf{A}$

exp $[i(\mathbf{k}\cdot\mathbf{x}-\omega t)]$, where **A** represents the amplitude and polarization of the plane wave, $\mathbf{k}=k_x\hat{\mathbf{x}}+k_y\hat{\mathbf{y}}+k_z\hat{\mathbf{z}}$ is its wave vector with Cartesian components k_x, k_y and k_z, $\mathbf{x}=x\hat{\mathbf{x}}+y\hat{\mathbf{y}}+z\hat{\mathbf{z}}$ is the position vector and ω denotes angular frequency. For plane P waves $\mathbf{A}\times\mathbf{k}=\mathbf{0}$ and $k=(k_x^2+k_y^2+k_z^2)^{1/2}=\omega/\alpha$, where α denotes the P-wave velocity, whereas for plane S waves $\mathbf{A}\cdot\mathbf{k}=0$ and $k=\omega/\beta$, where β denotes the S-wave velocity.

The objective of the PML method is to construct a new wave equation that permits plane-wave solutions of the form $\mathbf{A}\exp[i(\mathbf{k}\cdot\mathbf{x}-\omega t)-\gamma x]$, $\gamma>0$, i.e., plane waves that decay exponentially in the direction of increasing x, say, while ensuring a reflection coefficient between the medium and the PML region that is exactly zero for all angles of incidence and all frequencies before discretization. Following the discussion of Collino & Tsogka (2001), to which the reader is referred for more details, this may be accomplished by introducing a new variable $\tilde{x}=x-i\gamma$ and transforming the original eq. (1) in terms of variables x, y, z, to a new wave equation in terms of variables $\tilde{x}$, y, z, where we have defined the origin of coordinates $x=0$ at the contact between the regular domain and the PML layer, and the PML region corresponds to $x>0$ (see Fig. 1). This new wave equation permits plane-wave solutions of the desired form $\mathbf{A}\exp[i(k_x\tilde{x}+k_yy+k_zz-\omega t)]=\mathbf{A}\exp[i(\mathbf{k}\cdot\mathbf{x}-\omega t)-\gamma x]$. The key in this mapping is the choice of γ.

Suppose the normal to the interface between the model and the PML layer is given by $\hat{\mathbf{n}}$ (Fig. 1). We define the coordinate in the direction of increasing $\hat{\mathbf{n}}$ to be n. The gradient operator $\boldsymbol{\nabla}$ can now be split in terms of components perpendicular and parallel to the interface:

$$\boldsymbol{\nabla}=\hat{\mathbf{n}}\partial_n+\boldsymbol{\nabla}^{\parallel}, \tag{3}$$

where $\partial_n=\hat{\mathbf{n}}\cdot\boldsymbol{\nabla}$ and $\boldsymbol{\nabla}^{\parallel}=(\mathbf{I}-\hat{\mathbf{n}}\hat{\mathbf{n}})\cdot\boldsymbol{\nabla}$, where **I** is the 3×3 identity tensor, and $\mathbf{I}-\hat{\mathbf{n}}\hat{\mathbf{n}}$ is the projection operator on to the surface with normal $\hat{\mathbf{n}}$.

2.1 Classical PML formulation for first-order systems

In the classical first-order velocity-stress formulation, one first rewrites eq. (1) as

$$\begin{aligned}\rho\partial_t\mathbf{v}&=\boldsymbol{\nabla}\cdot\boldsymbol{\sigma},\\ \partial_t\boldsymbol{\sigma}&=\mathbf{c}:\boldsymbol{\nabla}\mathbf{v},\end{aligned} \tag{4}$$

where **v** is the velocity vector and $\boldsymbol{\sigma}$ is the second-order stress tensor. The frequency-domain form is

$$\begin{aligned}i\omega\rho\mathbf{v}&=\boldsymbol{\nabla}\cdot\boldsymbol{\sigma},\\ i\omega\boldsymbol{\sigma}&=\mathbf{c}:\boldsymbol{\nabla}\mathbf{v}.\end{aligned} \tag{5}$$

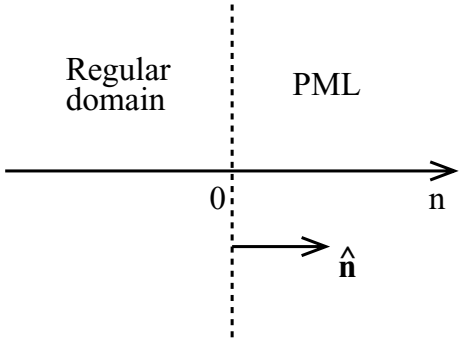

Figure 1. Definition of the regular domain and the PML region. The PML layer starts at $n=0$ and extends to $n>0$. The local normal to the interface is denoted by $\hat{\mathbf{n}}$.

Using eq. (3), one obtains

$$\begin{aligned}i\omega\rho\mathbf{v}&=\hat{\mathbf{n}}\partial_n\cdot\boldsymbol{\sigma}+\boldsymbol{\nabla}^{\parallel}\cdot\boldsymbol{\sigma},\\ i\omega\boldsymbol{\sigma}&=\mathbf{c}:\hat{\mathbf{n}}\partial_n\mathbf{v}+\mathbf{c}:\boldsymbol{\nabla}^{\parallel}\mathbf{v}.\end{aligned} \tag{6}$$

Next, one introduces a damping profile d across the PML region, such that $d=0$ inside the medium and $d>0$ in the PML, and a new complex coordinate $\tilde{n}$:

$$\tilde{n}(n)=n-\frac{i}{\omega}\int_0^n d(s)\,ds, \tag{7}$$

or, equivalently, upon differentiating

$$\frac{\partial n}{\partial\tilde{n}}=\frac{i\omega}{i\omega+d(n)}. \tag{8}$$

One then replaces the wave eq. (6) written in terms of n with a generalized wave equation written in terms of $\tilde{n}$:

$$\begin{aligned}i\omega\rho\mathbf{v}&=\hat{\mathbf{n}}\partial_{\tilde{n}}\cdot\boldsymbol{\sigma}+\boldsymbol{\nabla}^{\parallel}\cdot\boldsymbol{\sigma},\\ i\omega\boldsymbol{\sigma}&=\mathbf{c}:\hat{\mathbf{n}}\partial_{\tilde{n}}\mathbf{v}+\mathbf{c}:\boldsymbol{\nabla}^{\parallel}\mathbf{v}.\end{aligned} \tag{9}$$

Inside the medium, both equations are identical because $d=0$. However, in the PML, this modified wave equation permits exponentially decaying plane-wave solutions in the $\hat{\mathbf{n}}$ direction. Note that the choice of decay is $\gamma=\omega^{-1}\int_0^n d(s)\,ds$, and that it is inversely proportional to the angular frequency ω of the plane wave. One then uses the mapping (7) to rewrite the wave equation (9) in terms of n rather than $\tilde{n}$:

$$\begin{aligned}i\omega\rho\mathbf{v}&=\hat{\mathbf{n}}(\partial n/\partial\tilde{n})\partial_n\cdot\boldsymbol{\sigma}+\boldsymbol{\nabla}^{\parallel}\cdot\boldsymbol{\sigma},\\ i\omega\boldsymbol{\sigma}&=\mathbf{c}:\hat{\mathbf{n}}(\partial n/\partial\tilde{n})\partial_n\mathbf{v}+\mathbf{c}:\boldsymbol{\nabla}^{\parallel}\mathbf{v}.\end{aligned} \tag{10}$$

Note that we have not had to assume that the interface is aligned with a coordinate axis, i.e., this PML formulation works in curvilinear coordinates (Collino & Monk 1998b). Next, using the split-field technique (e.g. Chew & Weedon 1994; Collino & Monk 1998b), one splits the velocity and the stress into two parts, $\mathbf{v}=\mathbf{v}^1+\mathbf{v}^2$ and $\boldsymbol{\sigma}=\boldsymbol{\sigma}^1+\boldsymbol{\sigma}^2$, such that

$$\begin{aligned}i\omega\rho\mathbf{v}^1&=(\partial n/\partial\tilde{n})\hat{\mathbf{n}}\cdot\partial_n\boldsymbol{\sigma},\\ i\omega\rho\mathbf{v}^2&=\boldsymbol{\nabla}^{\parallel}\cdot\boldsymbol{\sigma},\\ i\omega\boldsymbol{\sigma}^1&=(\partial n/\partial\tilde{n})\mathbf{c}:\hat{\mathbf{n}}\partial_n\mathbf{v},\\ i\omega\boldsymbol{\sigma}^2&=\mathbf{c}:\boldsymbol{\nabla}^{\parallel}\mathbf{v}.\end{aligned} \tag{11}$$

Substituting (8) in (11) and converting back to the time domain we obtain

$$\begin{aligned}(\partial_t+d)\rho\mathbf{v}^1&=\hat{\mathbf{n}}\partial_n\cdot\boldsymbol{\sigma},\\ \partial_t\rho\mathbf{v}^2&=\boldsymbol{\nabla}^{\parallel}\cdot\boldsymbol{\sigma},\\ (\partial_t+d)\boldsymbol{\sigma}^1&=\mathbf{c}:\hat{\mathbf{n}}\partial_n\mathbf{v},\\ \partial_t\boldsymbol{\sigma}^2&=\mathbf{c}:\boldsymbol{\nabla}^{\parallel}\mathbf{v}.\end{aligned} \tag{12}$$

Eq. (12) permits the desired exponentionally decaying plane-wave solutions and governs wave propagation in the classical first-order PML.

2.2 Second-order systems

The key idea in this article is that we can apply the same concept to the wave equation formulated as a second-order system in displacement. Based upon the splitting of the gradient operator (3), eq. (2) can first be rewritten as

$$\begin{aligned}-\rho\omega^2\mathbf{s}=\hat{\mathbf{n}}\partial_n\cdot(\mathbf{c}:\hat{\mathbf{n}}\partial_n\mathbf{s})+\hat{\mathbf{n}}\partial_n\cdot(\mathbf{c}:\boldsymbol{\nabla}^{\parallel}\mathbf{s})\\ +\boldsymbol{\nabla}^{\parallel}\cdot(\mathbf{c}:\hat{\mathbf{n}}\partial_n\mathbf{s})+\boldsymbol{\nabla}^{\parallel}\cdot(\mathbf{c}:\boldsymbol{\nabla}^{\parallel}\mathbf{s}).\end{aligned} \tag{13}$$

Introducing the new complex coordinate $\tilde{n}$ as defined by eq. (7), we obtain

$$-\rho\omega^2\mathbf{s} = \hat{\mathbf{n}}\partial_{\tilde{n}}\cdot(\mathbf{c}:\hat{\mathbf{n}}\partial_{\tilde{n}}\mathbf{s}) + \hat{\mathbf{n}}\partial_{\tilde{n}}\cdot(\mathbf{c}:\boldsymbol{\nabla}^{\parallel}\mathbf{s}) + \boldsymbol{\nabla}^{\parallel}\cdot(\mathbf{c}:\hat{\mathbf{n}}\partial_{\tilde{n}}\mathbf{s}) + \boldsymbol{\nabla}^{\parallel}\cdot(\mathbf{c}:\boldsymbol{\nabla}^{\parallel}\mathbf{s}). \quad (14)$$

Using the mapping (7), we now rewrite the wave equation (14) in terms of n rather than $\tilde{n}$:

$$-\rho\omega^2\mathbf{s} = \hat{\mathbf{n}}\partial_n\cdot(\mathbf{c}:\hat{\mathbf{n}}\partial_n\mathbf{s})(\partial n/\partial\tilde{n})^2 + \hat{\mathbf{n}}\cdot(\mathbf{c}:\hat{\mathbf{n}}\partial_n\mathbf{s})(\partial n/\partial\tilde{n})\partial_n(\partial n/\partial\tilde{n}) + [\hat{\mathbf{n}}\partial_n\cdot(\mathbf{c}:\boldsymbol{\nabla}^{\parallel}\mathbf{s}) + \boldsymbol{\nabla}^{\parallel}\cdot(\mathbf{c}:\hat{\mathbf{n}}\partial_n\mathbf{s})](\partial n/\partial\tilde{n}) + \boldsymbol{\nabla}^{\parallel}\cdot(\mathbf{c}:\boldsymbol{\nabla}^{\parallel}\mathbf{s}). \quad (15)$$

Next, we split the displacement into four parts

$$\mathbf{s} = \mathbf{s}^1 + \mathbf{s}^2 + \mathbf{s}^3 + \mathbf{s}^4, \quad (16)$$

such that

$$\begin{aligned}
-\rho\omega^2\mathbf{s}^1 &= \hat{\mathbf{n}}\partial_n\cdot(\mathbf{c}:\hat{\mathbf{n}}\partial_n\mathbf{s})(\partial n/\partial\tilde{n})^2,\\
-\rho\omega^2\mathbf{s}^2 &= \hat{\mathbf{n}}\cdot(\mathbf{c}:\hat{\mathbf{n}}\partial_n\mathbf{s})(\partial n/\partial\tilde{n})\partial_n(\partial n/\partial\tilde{n}),\\
-\rho\omega^2\mathbf{s}^3 &= [\hat{\mathbf{n}}\partial_n\cdot(\mathbf{c}:\boldsymbol{\nabla}^{\parallel}\mathbf{s}) + \boldsymbol{\nabla}^{\parallel}\cdot(\mathbf{c}:\hat{\mathbf{n}}\partial_n\mathbf{s})](\partial n/\partial\tilde{n}),\\
-\rho\omega^2\mathbf{s}^4 &= \boldsymbol{\nabla}^{\parallel}\cdot(\mathbf{c}:\boldsymbol{\nabla}^{\parallel}\mathbf{s}).
\end{aligned} \quad (17)$$

Upon differentiating eq. (8) we find that

$$\frac{\partial}{\partial n}\left(\frac{\partial n}{\partial\tilde{n}}\right) = -\frac{i\omega}{(i\omega+d)^2}d'(n). \quad (18)$$

Substituting this and eq. (8) in eq. (17) and converting back to the time domain we obtain

$$\begin{aligned}
\rho(\partial_t+d)^2\mathbf{s}^1 &= \hat{\mathbf{n}}\partial_n\cdot(\mathbf{c}:\hat{\mathbf{n}}\partial_n\mathbf{s}),\\
\rho(\partial_t+d)^3\mathbf{s}^2 &= -d'\hat{\mathbf{n}}\cdot(\mathbf{c}:\hat{\mathbf{n}}\partial_n\mathbf{s}),\\
\rho\partial_t(\partial_t+d)\mathbf{s}^3 &= \hat{\mathbf{n}}\partial_n\cdot(\mathbf{c}:\boldsymbol{\nabla}^{\parallel}\mathbf{s}) + \boldsymbol{\nabla}^{\parallel}\cdot(\mathbf{c}:\hat{\mathbf{n}}\partial_n\mathbf{s}),\\
\rho\partial_t^2\mathbf{s}^4 &= \boldsymbol{\nabla}^{\parallel}\cdot(\mathbf{c}:\boldsymbol{\nabla}^{\parallel}\mathbf{s}).
\end{aligned} \quad (19)$$

Eq. (9) also permits the desired exponentially decaying plane-wave solutions and governs wave propagation in the PML formulated in displacement. Note that we have obtained a third-order system in time, in contrast to the classical first-order velocity-stress formulation (12). In many numerical schemes, it is simpler to rewrite it as a second-order system using an intermediate variable

$$\mathbf{t} = (\partial_t + d)\mathbf{s}^2 \quad (20)$$

such that eq. (19) becomes

$$\begin{aligned}
\rho(\partial_t+d)^2\mathbf{s}^1 &= \hat{\mathbf{n}}\partial_n\cdot(\mathbf{c}:\hat{\mathbf{n}}\partial_n\mathbf{s}),\\
\rho(\partial_t+d)^2\mathbf{t} &= -d'\hat{\mathbf{n}}\cdot(\mathbf{c}:\hat{\mathbf{n}}\partial_n\mathbf{s}),\\
\rho\partial_t(\partial_t+d)\mathbf{s}^3 &= \hat{\mathbf{n}}\partial_n\cdot(\mathbf{c}:\boldsymbol{\nabla}^{\parallel}\mathbf{s}) + \boldsymbol{\nabla}^{\parallel}\cdot(\mathbf{c}:\hat{\mathbf{n}}\partial_n\mathbf{s}),\\
\rho\partial_t^2\mathbf{s}^4 &= \boldsymbol{\nabla}^{\parallel}\cdot(\mathbf{c}:\boldsymbol{\nabla}^{\parallel}\mathbf{s}).
\end{aligned} \quad (21)$$

The main drawback of eq. (21) is that one needs to modify existing numerical codes in order to handle the first-order system (20), i.e. an Euler or a Runge–Kutta time scheme has to be used, in addition to the classical explicit finite-difference time schemes used for the other variables $\mathbf{s}^1$, $\mathbf{s}^3$ and $\mathbf{s}^4$. For instance, the four terms in eq. (21) can be marched based upon an explicit Newmark scheme (e.g. Hughes 1987), evaluating the terms on the right-hand side at the current time step, and discretizing the second-order time operators on the left-hand side $(\partial_t+d)^2$, $\partial_t(\partial_t+d)$ and $\partial^2{}_t$ explicitly. One can then use a first-order scheme to march eq. (20) explicitly as well by discretizing (∂_t+d) to obtain $\mathbf{s}^2$ from the known value of $\mathbf{t}$ computed in eq. (21). The total displacement vector $\mathbf{s}$ can then be computed by summing the known values of $\mathbf{s}^1$, $\mathbf{s}^2$, $\mathbf{s}^3$ and $\mathbf{s}^4$ according to eq. (16).

Another drawback of the PML in general (either as a first-order or as a second-order system) is that additional memory is required to store the split-field arrays. However, this applies to the PML region only, which, because of the efficiency of the PML, is small compared with the main model, therefore in practice this problem is negligible. It is worth mentioning in this regard that in the context of electromagnetics an alternative 'anisotropic' PML formulation has been introduced to overcome this problem (e.g. Sacks *et al.* 1995; Zhao & Cangellaris 1996). How this formulation could be used in elastodynamics remains to be studied.

In order to use this PML system in the context of techniques such as the finite-element or spectral-element methods, one needs to write a variational formulation of the problem. The 'weak' or variational form of the classical wave eq. (1) is obtained by dotting it with any test vector $\mathbf{w}$ and integrating by parts over the volume V of the domain:

$$\int_{\mathrm{V}}\rho\mathbf{w}\cdot\partial_t^2\mathbf{s}\,d^3\mathbf{r} = -\int_{\mathrm{V}}(\boldsymbol{\nabla}\mathbf{w}):\mathbf{c}:(\boldsymbol{\nabla}\mathbf{s})d^3\mathbf{r}, \quad (22)$$

where we have used the free surface boundary condition and the fact that the match with the PML layer is 'perfect', i.e. on the boundary between the PML region and the regular domain the respective wave equations are identical. Similarly, the weak form of the PML system, eq. (21), is

$$\begin{aligned}
\int_{\mathrm{V}}\rho(\partial_t+d)^2\mathbf{s}^1\cdot\mathbf{w}\,d^3\mathbf{r} &= -\int_{\mathrm{V}}(\hat{\mathbf{n}}\partial_n\mathbf{w}):\mathbf{c}:(\hat{\mathbf{n}}\partial_n\mathbf{s})\,d^3\mathbf{r} + \int_{\Gamma}\hat{\mathbf{n}}\mathbf{w}:\mathbf{c}:(\hat{\mathbf{n}}\partial_n\mathbf{s})\,d^2\mathbf{r},\\
\int_{\mathrm{V}}\rho(\partial_t+d)^2\mathbf{t}\cdot\mathbf{w}\,d^3\mathbf{r} &= -\int_{\mathrm{V}}d'\hat{\mathbf{n}}\mathbf{w}:\mathbf{c}:(\hat{\mathbf{n}}\partial_n\mathbf{s})\,d^3\mathbf{r},\\
\int_{\mathrm{V}}\rho\partial_t(\partial_t+d)\mathbf{s}^3\cdot\mathbf{w}\,d^3\mathbf{r} &= -\int_{\mathrm{V}}\big[(\hat{\mathbf{n}}\partial_n\mathbf{w}):\mathbf{c}:(\boldsymbol{\nabla}^{\parallel}\mathbf{s}) + (\boldsymbol{\nabla}^{\parallel}\mathbf{w}):\mathbf{c}:(\hat{\mathbf{n}}\partial_n\mathbf{s})\big]\,d^3\mathbf{r} + \int_{\Gamma}\hat{\mathbf{n}}\mathbf{w}:\mathbf{c}:(\boldsymbol{\nabla}^{\parallel}\mathbf{s})\,d^2\mathbf{r},\\
\int_{\mathrm{V}}\rho\partial_t^2\mathbf{s}^4\cdot\mathbf{w}\,d^3\mathbf{r} &= -\int_{\mathrm{V}}(\boldsymbol{\nabla}^{\parallel}\mathbf{w}):\mathbf{c}:(\boldsymbol{\nabla}^{\parallel}\mathbf{s})\,d^3\mathbf{r}.
\end{aligned} \quad (23)$$

Again the match with the regular domain is assumed to be perfect. The boundary Γ denotes the surface of the PML that is not in contact with the regular domain.

We note that a very similar second-order PML system could be written for the acoustic wave equation formulated either in pressure or using a generalized potential (Komatitsch & Tromp 2002). This would allow one to use the PML in the context of fluid-solid simulations.

3 NUMERICAL VALIDATION

To illustrate the efficiency of the PML system, eqs (20) and (21), we simulate the propagation of P–SV waves in a 2-D elastic isotropic homogeneous medium. The medium is a block with P velocity $\alpha = 2000\ \mathrm{m\cdot s^{-1}}$ and S velocity $\beta = 1154.7\ \mathrm{m\cdot s^{-1}}$, which corresponds to a value of 0.25 for Poisson's ratio, and density $\rho = 2200\ \mathrm{kg\ m^{-3}}$. The size of the model is 30 m × 30 m. The source time function is a Ricker wavelet, i.e. the second derivative of a Gaussian, with a dominant frequency of 1000 Hz.

We first want to validate the PML condition for surface waves. Therefore, we place the source, which is a vertical force, very close to the surface at a depth of 1.5 m and a horizontal distance of 3 m from the centre of the block, in order to generate a large incident Rayleigh wave. A receiver is located on the surface at a horizontal distance of 10.5 m from the centre of the block, and records the two components of displacement. On the two vertical edges of the

finite-size medium, PML absorbing conditions are imposed in order to mimic a half-space. We do not use the PML at the bottom of the mesh for simplicity because we stop the simulation before waves can come back to the receiver.

We choose to compute synthetic seismograms based upon the spectral-element method because it has proven to be very precise in the context of elastic wave propagation, with very little numerical dispersion, and also because the free surface boundary condition is automatically taken into account, which means that surface waves are very accurately modelled (Komatitsch & Tromp 1999, 2002).

The model is discretized using 60×60 spectral elements, and we use a polynomial degree $N = 5$ in each element, which means that the entire model contains a total of $(60N + 1)^2 = 90\ 601$ Gauss–Lobatto–Legendre gridpoints (for details on the spectral-element method, the reader is referred to Komatitsch & Tromp 1999, 2002). The PML region consists of two layers of spectral elements, and therefore contains $2N + 1 = 11$ Gauss–Lobatto–Legendre

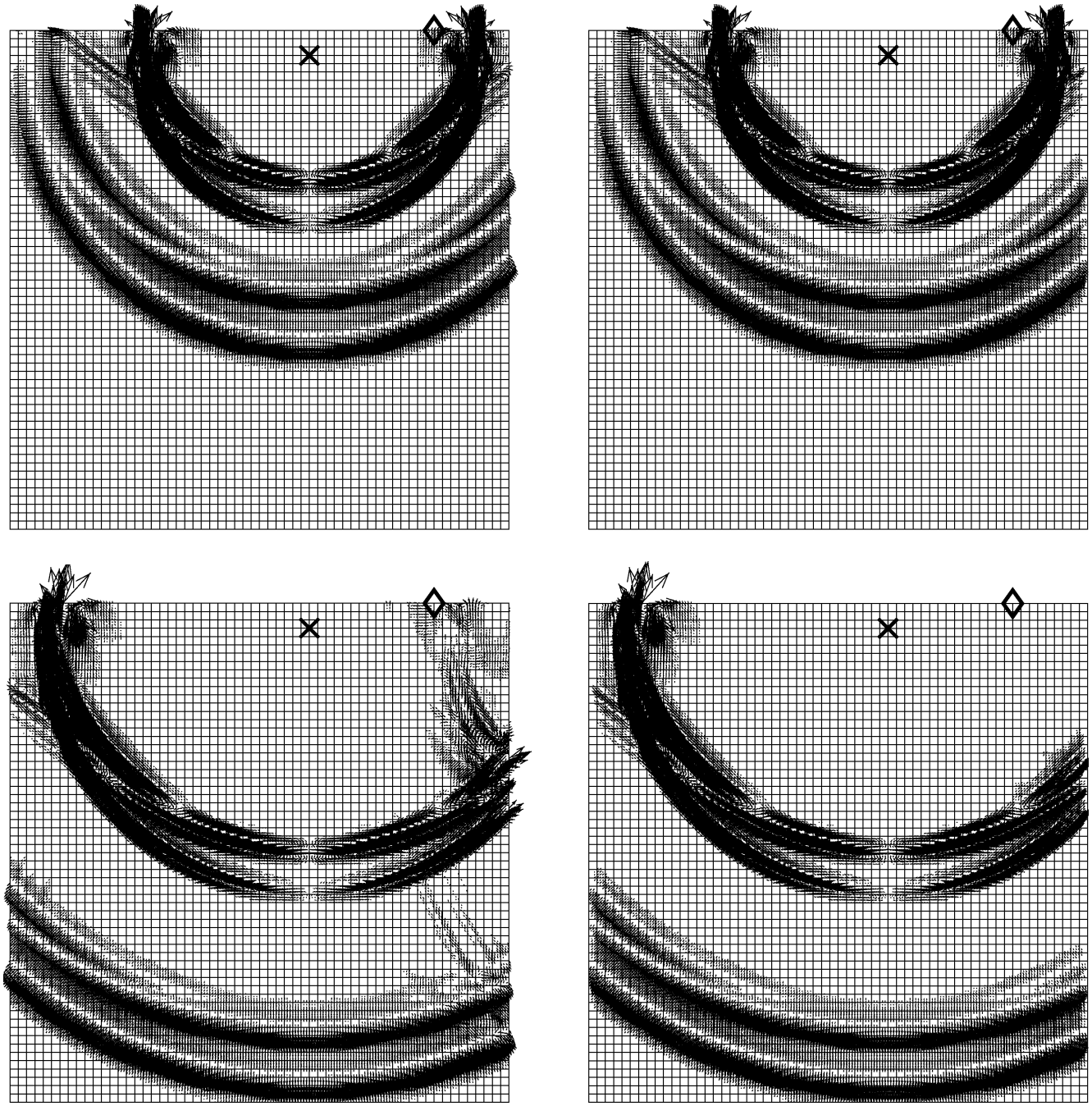

Figure 2. Snapshots of a spectral-element simulation for surface waves at time $t = 10$ ms (top) and $t = 15$ ms (bottom), using the 'A1' paraxial treatment of Clayton & Engquist (1977) (left) and the PML (right). The small arrows represent the displacement vector. The grid cells represent the spectral elements. Each element contains $(N + 1)^2 = 36$ Gauss–Lobatto–Legendre gridpoints. The cross indicates the position of the vertical force and the diamond indicates the receiver. The display has been truncated below 1 per cent of the maximum amplitude of the wavefield, with the same graphical normalization factor used for both tests. One can clearly see that the PML condition is more efficient, in particular for the Rayleigh wave, as well as for body waves with non-normal incidence (bottom).

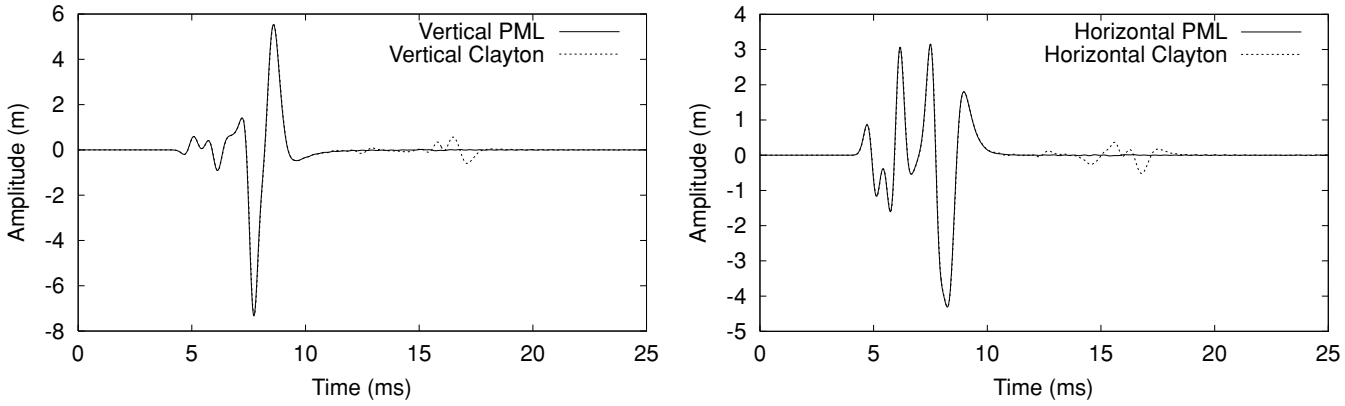

Figure 3. Vertical (left) and horizontal (right) components of displacement recorded on the surface at the receiver denoted by the diamond in Fig. 2, using the PML (solid line) and the 'A1' paraxial condition of Clayton & Engquist (1977) (dashed line). In the case of the PML, there is almost no spurious wave reflected off the boundary, while in the case of the paraxial treatment, a large signal is recorded.

grid points in the damping direction. At the bottom of the PML, i.e. on the edge of the grid, we impose Dirichlet boundary conditions (zero displacement). The time step is 10 μs and the total duration of the simulation is 25 ms. In the PML, we use the empirical damping profile

$$d(x) = \frac{3\alpha}{2\delta} \log\left(\frac{1}{R}\right) \left(\frac{x}{\delta}\right)^2, \tag{24}$$

which is used by many authors, e.g. Collino & Tsogka (2001), where δ is the width of the PML layer, x is the horizontal coordinate with the origin chosen at the top of the PML layer and R is the theoretical reflection coefficient after discretization, which can be chosen to be very small (typically 10^{-3}, which is the value used in this article).

In Fig. 2, we compare snapshots obtained using the PML condition and the so-called 'A1' paraxial condition of Clayton & Engquist (1977). The large Rayleigh wave can easily be identified based upon its elliptical polarization. The PML is clearly superior in terms of absorbing both body and surface waves; in particular, in regions of the mesh where the waves are not incident close to the normal to the boundary. The efficiency of the paraxial condition for body waves is not satisfactory when the angle of incidence differs from 90°, as can be seen in particular in the bottom part of the last snapshot; it also behaves poorly for surface waves, as expected from the fact that the polarization of the Rayleigh wave is elliptical, and a significant part of the incident energy is reflected back into the model. More sophisticated paraxial conditions could have been used as a reference (e.g. Higdon 1991 or Quarteroni *et al.* 1998), but Collino & Tsogka (2001) demonstrated than Higdon (1991) is far less efficient than the classical first-order PML.

Fig. 3 shows the seismogram recorded at the receiver at the surface. Because it is located on the surface, it mostly records a large-amplitude Rayleigh wave, in addition to the smaller direct body waves. In the case of the simulation with the Clayton & Engquist (1977) boundary condition, a large spurious signal is reflected off the boundary, while in the case of the PML, this unwanted reflection is almost completely suppressed.

Next, we validate the efficiency of the PML for body waves in a medium with a high value of Poisson's ratio. Low values of Poisson's ratio have already been shown to be stable and accurate in the context of the PML by Collino & Tsogka (2001), but high values are known for creating stability issues in some classical paraxial absorbing boundary conditions (Clayton & Engquist 1977; Stacey 1988; Mahrer 1990). Therefore, it is of interest to test such high values.

We change the S velocity of the medium to $\beta = 880$ m s^{-1}, which corresponds to a value of 0.38 for Poisson's ratio. We also change the size of the model to 15 m × 60 m, and discretize it using 30 × 120 spectral elements, i.e. a total of $(30N + 1) \times (120N + 1) = 90\,751$ Gauss–Lobatto–Legendre gridpoints. We place the source at $x_s = 4.5$ m and $z_s = 24$ m, and the receiver in $x_r = 12$ m and $z_r = 33$ m (see Fig. 4). To avoid numerical dispersion related to the high value of Poisson's ratio, and the related short S wavelength, we reduce the dominant frequency of the Ricker source to 900 Hz. The other parameters of the simulation are unchanged. In Fig. 4, the snapshots obtained using the PML condition show that the condition is stable and efficient for both P and S waves, while the paraxial condition of Clayton & Engquist (1977) is stable but reflects a significant amount of spurious energy into the domain. The seismogram of Fig. 5 confirms that the PML condition is superior and exhibits very high efficiency.

CONCLUSIONS

We formulated a PML condition for the elastic wave equation written as a second-order system in displacement. This allows one to use the PML in the context of numerical techniques such as the finite-element method, the spectral-element method and second-order finite-difference methods. The excellent efficiency of the condition was demonstrated using 2-D benchmarks for body and surface waves. The condition was observed to be stable for a wide range of values of Poisson's ratio, including high values that can create stability issues in the case of other classical absorbing boundary conditions.

We did not change the basic idea behind the PML, but simply reformulated the classical first-order condition. Therefore, we expect to find the same properties as in the classical PML, i.e. use of the formulation for 3-D problems is straightforward (e.g. Bérenger 1996; Chew & Liu 1996), and the case of the corners of the model can be handled by combining different PMLs written along different grid axes (e.g. Bérenger 1994; Collino & Tsogka 2001).

However, we also find the same limitations as with the classical first-order PML. First, at grazing incidence the behaviour of the discrete PML is poor, and the associated numerical reflection coefficient is high (Collino & Monk 1998a; Winton & Rappaport 2000). Following the work of these authors, one can numerically optimize the damping profile of eq. (24) in order to optimize the behaviour at

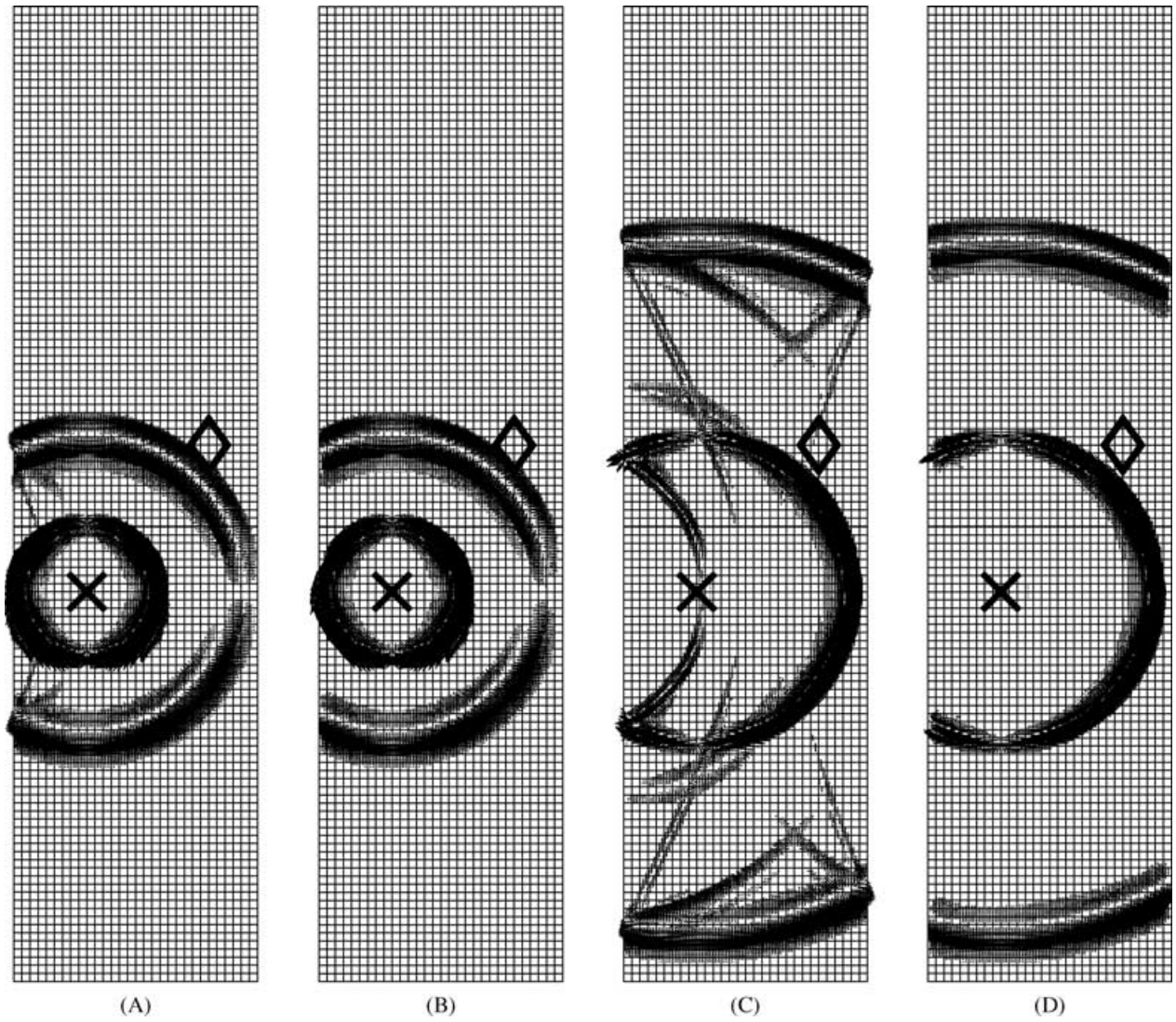

Figure 4. Snapshots of a spectral-element simulation for body waves at time $t = 6$ ms (A and B, left) and $t = 12$ ms (C and D, right), using the 'A1' paraxial treatment of Clayton & Engquist (1977) (A and C) and the PML (B and D). The small arrows represent the displacement vector. The grid cells represent the spectral elements. Each element contains $(N + 1)^2 = 36$ Gauss–Lobatto–Legendre gridpoints. The cross indicates the position of the vertical force and the diamond indicates the receiver. The display has been truncated below 1 per cent of the maximum amplitude of the wavefield, with the same graphical normalization factor used for both tests. One can clearly see that the PML condition is more efficient for both P and S waves.

grazing incidence. Secondly, as noted by Bécache *et al.* (2003), for some anisotropic media intrinsic instabilities appear, even though it could seem from eqs (2) and (13) that any anisotropic elastic tensor could be used.

Let us finally mention that, in addition to seismic wave propagation, the second-order implementation of the PML method introduced in this article could be applied in the context of other second-order equations.

ACKNOWLEDGMENTS

The authors would like to thank Chrysoula Tsogka and Roland Martin for fruitful discussions, and Peter Moczo and an anonymous reviewer for useful comments. This material is based in part upon work supported by the National Science Foundation. This is contribution no 8888 of the Division of Geological & Planetary Sciences of the California Institute of Technology.

REFERENCES

Bao, H., Bielak, J., Ghattas, O., Kallivokas, L.F., O'Hallaron, D.R., Shewchuk, J.R. & Xu, J., 1998. Large-scale simulation of elastic wave propagation in heterogeneous media on parallel computers, *Comput. Methods Appl. Mech. Eng.,* **152,** 85–102.

Basu, U. & Chopra, A.K., 2003. Perfectly matched layers for time-harmonic elastodynamics of unbounded domains: theory and finite-element implementation, *Comput. Methods Appl. Mech. Eng.,* **192,** 1337–1375.

Bécache, E., Fauqueux, S. & Joly, P., 2003. Stability of perfectly matched layers, group velocities and anisotropic waves, *J. Comput. Phys.*, in press.

Bérenger, J.P., 1994. A perfectly matched layer for the absorption of electromagnetic waves, *J. Comput. Phys.,* **114,** 185–200.

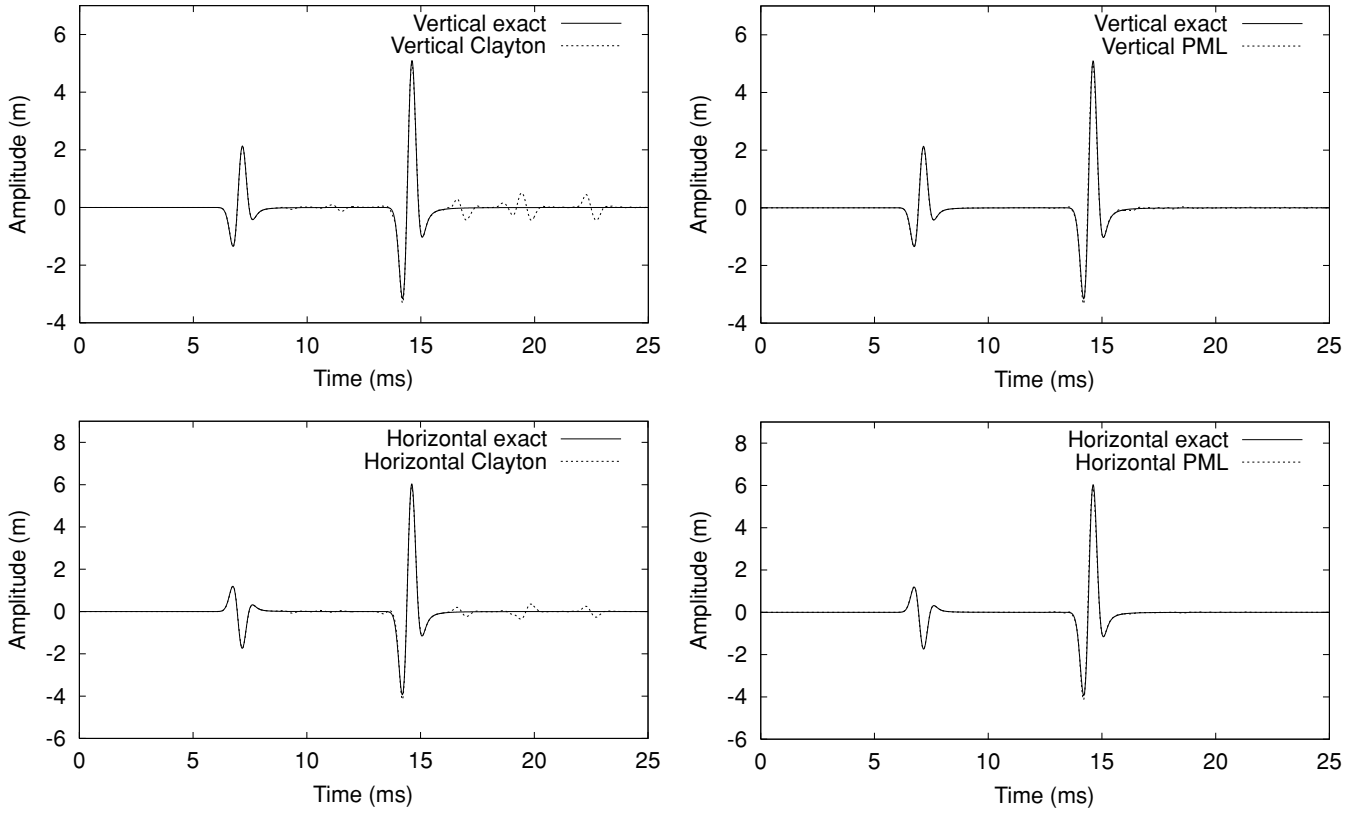

Figure 5. Vertical (top) and horizontal (bottom) components of displacement recorded at the receiver denoted by the diamond in Fig. 4, using the 'A1' paraxial condition of Clayton & Engquist (1977) (left, dashed line) and the PML (right, dashed line), compared with the analytical solution of the problem, i.e. Green's function for a 2-D homogeneous unbounded medium (solid line). In the case of the PML, there is almost no spurious wave reflected off the boundary, while in the case of the paraxial treatment, large spurious arrivals are recorded both after the P and after the S wave. A small amount of numerical dispersion can be seen in both cases because of the short S wavelength related to the high value of Poisson's ratio.

Bérenger, J.P., 1996. Three-dimensional perfectly matched layer for the absorption of electromagnetic waves, *J. Comput. Phys.,* **127,** 363–379.

Cerjan, C., Kosloff, D., Kosloff, R. & Reshef, M., 1985. A nonreflecting boundary condition for discrete acoustic and elastic wave equation, *Geophysics,* **50,** 705–708.

Chew, W.C. & Liu, Q., 1996. Perfectly matched layers for elastodynamics: a new absorbing boundary condition, *J. Comput. Acoust.,* **4,** 341–359.

Chew, W.C. & Weedon, W.H., 1994. A 3-D perfectly matched medium from modified Maxwell's equations with stretched coordinates, *Microwave Opt. Technol. Lett.,* **7,** 599–604.

Clayton, R. & Engquist, B., 1977. Absorbing boundary conditions for acoustic and elastic wave equations, *Bull. seism. Soc. Am.,* **67,** 1529–1540.

Collino, F. & Monk, P., 1998a. Optimizing the perfectly matched layer, *Comput. Methods Appl. Mech. Eng.,* **164,** 157–171.

Collino, F. & Monk, P., 1998b. The perfectly matched layer in curvilinear coordinates, *SIAM J. Sci. Comput.,* **19,** 2061–2090.

Collino, F. & Tsogka, C., 2001. Application of the PML absorbing layer model to the linear elastodynamic problem in anisotropic heterogeneous media, *Geophysics,* **66,** 294–307.

Engquist, B. & Majda, A., 1977. Absorbing boundary conditions for the numerical simulation of waves, *Math. Comp.,* **31,** 629–651.

Cohen, G. & Fauqueux, S., 2003. Mixed spectral finite elements for the linear elasticity system in unbounded domains, *SIAM J. Sci. Comput.,* in press.

Givoli, D., 1991. Non-reflecting boundary conditions: review article, *J. Comput. Phys.,* **94,** 1–29.

Grote, M.J., 2000. Nonreflecting boundary conditions for elastodynamics scattering, *J. Comput. Phys.,* **161,** 331–353.

Hagstrom, T., 1999. Radiation boundary conditions for the numerical simulation of waves, *Acta Numerica,* **8,** 47–106.

Hagstrom, T. & Hariharan, S.I., 1998. A formulation of asymptotic and exact boundary conditions using local operators, *Appl. Num. Math.,* **27,** 403–416.

Hastings, F.D., Schneider, J.B. & Broschat, S.L., 1996. Application of the perfectly matched layer (PML) absorbing boundary condition to elastic wave propagation, *J. Acoust. Soc. Am.,* **100,** 3061–3069.

Hesthaven, J.S., 1998. On the analysis and construction of perfectly matched layers for the linearized Euler equations, *J. Comput. Phys.,* **142,** 129–147.

Higdon, R.L., 1991. Absorbing boundary conditions for elastic waves, *Geophysics,* **56,** 231–241.

Hughes, T.J.R., 1987. *The Finite Element Method, Linear Static and Dynamic Finite Element Analysis*, Prentice-Hall, Englewood Cliffs.

Komatitsch, D. & Tromp, J., 1999. Introduction to the spectral-element method for 3-D seismic wave propagation, *Geophys. J. Int.,* **139,** 806–822.

Komatitsch, D. & Tromp, J., 2002. Spectral-element simulations of global seismic wave propagation—I. Validation, *Geophys. J. Int.,* **149,** 390–412.

Komatitsch, D. & Vilotte, J.P., 1998. The spectral-element method: an efficient tool to simulate the seismic response of 2D and 3D geological structures, *Bull. seism. Soc. Am.,* **88,** 368–392.

Kosmanis, T.I., Yioultsis, T.V. & Tsiboukis, T.D., 1999. Perfectly matched anisotropic layer for the numerical analysis of unbounded eddy-current problems, *IEEE Trans. Magn.,* **35,** 4452–4458.

Liu, Q. & Tao, J., 1997. The perfectly matched layer for acoustic waves in absorptive media, *J. Acoust. Soc. Am.,* **102,** 2072–2082.

Mahrer, K.D., 1990. Numerical time step instability and Stacey's and Clayton–Engquist's absorbing boundary conditions, *Bull. seism. Soc. Am.,* **80,** 213–217.

Moczo, P., Kristek, J. & Bystrický, E., 2001. Efficiency and optimization of the 3-D finite-difference modeling of seismic ground motion, *J. Comput. Acoust.,* **9,** 593–609.

Peng, C.B. & Töksoz, M.N., 1995. An optimal absorbing boundary condition for elastic wave modeling, *Geophysics,* **60,** 296–301.

Qi, Q. & Geers, T.L., 1998. Evaluation of the perfectly matched layer for computational acoustics, *J. Comput. Phys.,* **139,** 166–183.

Quarteroni, A., Tagliani, A. & Zampieri, E., 1998. Generalized Galerkin approximations of elastic waves with absorbing boundary conditions, *Comput. Methods Appl. Mech. Eng.,* **163,** 323–341.

Sacks, Z.S., Kingsland, D.M., Lee, R. & Lee, J.F., 1995. A perfectly matched anisotropic absorber for use as an absorbing boundary condition, *IEEE Trans. Antennas Propag.,* **43,** 1460–1463.

Sochacki, J., Kubichek, R., George, J., Fletcher, W.R. & Smithson, S., 1987. Absorbing boundary conditions and surface waves, *Geophysics,* **52,** 60–71.

Stacey, R., 1988. Improved transparent boundary formulations for the elastic wave equation, *Bull. seism. Soc. Am.,* **78,** 2089–2097.

Winton, S.C. & Rappaport, C.M., 2000. Specifying PML conductivities by considering numerical reflection dependencies, *IEEE Trans. Antennas Propag.,* **48,** 1055–1063.

Zeng, Y.Q., He, J.Q. & Liu, Q.H., 2001. The application of the perfectly matched layer in numerical modeling of wave propagation in poroelastic media, *Geophysics,* **66,** 1258–1266.

Zhao, L. & Cangellaris, A.C., 1996. GT-PML: generalized theory of perfectly matched layers and its application to the reflectionless truncation of finite-difference time-domain grids, *IEEE Trans. Microwave Theory Techn.,* **44,** 2555–2563.